OPEN ACCESS
IOP Publishing
Journal of Physics A: Mathematical and Theoretical
J. Phys. A: Math. Theor. **55** (2022) 484005 (15pp)
https://doi.org/10.1088/1751-8121/aca6b8

Quantum spin dynamics of quasi-one-dimensional Heisenberg-Ising magnets in a transverse field: confined spinons, E_8 spectrum, and quantum phase transitions

Kirill Amelin[1,*], Johan Viirok[1], Urmas Nagel[1], Toomas Rõõm[1], Johannes Engelmayer[2], Tusharkanti Dey[2,3], Agustinus Agung Nugroho[2,4], Thomas Lorenz[2] and Zhe Wang[5,*]

[1] National Institute of Chemical Physics and Biophysics, 12618 Tallinn, Estonia
[2] Institute of Physics II, University of Cologne, 50937 Cologne, Germany
[3] Department of Physics, Indian Institute of Technology (Indian School of Mines), Dhanbad 826004, Jharkhand, India
[4] Faculty of Mathematics and Natural Sciences, Institut Teknologi Bandung, 40132 Bandung, Indonesia
[5] Department of Physics, TU Dortmund University, 44227 Dortmund, Germany

E-mail: kirill.amelin@kbfi.ee and zhe.wang@tu-dortmund.de

Received 16 August 2022; revised 20 October 2022
Accepted for publication 28 November 2022
Published 7 December 2022

Abstract

We report on high-resolution terahertz spectroscopic studies of quantum spin dynamics in the quasi-one-dimensional Ising-like ferromagnet $CoNb_2O_6$ and antiferromagnet $BaCo_2V_2O_8$ as a function of an applied transverse magnetic field. In the ordered phases stabilized by inter-chain couplings, we reveal characteristics for confined spinon excitations, E_8 dynamical spectrum, and field-induced quantum phase transitions. The connections between these

* Authors to whom any correspondence should be addressed.

characteristic dynamical features are found in the field-dependent evolution of the excitation spectra.

Keywords: confined spinons, Heisenberg-Ising spin chain, transverse-field Ising-chain quantum critical point, E_8 dynamical spectrum, quantum phase transition, quantum spin dynamics

(Some figures may appear in colour only in the online journal)

1. Introduction

The one-dimensional (1D) quantum spin models are a subject of a constant stream of theoretical studies [1–6]. Despite their apparent simplicity, the spin-chain models exhibit a rich spectrum of fascinating physics, such as quantum phase transitions [2, 7–9], fractionalization [6, 10–12], complex bound states [13, 14], and quantum information [4]. It is possible to achieve an exact understanding of the physics, since the 1D models are analytically or numerically solvable. Invented over a century ago, the spin-1/2 Ising chain is a celebrated 1D model [15–17]. This model exhibits a long-range order only at zero temperature and a spin excitation gap in zero magnetic field. In an applied transverse field, the spin gap is reduced and finally closed at a critical field $B_{\perp}^{c,1\mathrm{D}}$ (see figure 1). A quantum phase transition occurs at the critical field, above which the long-range order is suppressed and the system enters the paramagnetic phase again with a finite spin gap.

An experimental realization and investigation of the Ising spin-chain model in a solid-state material is not straightforward. In a real material, it is not natural to have an infinite Ising anisotropy, but rather a finite one in addition to a Heisenberg isotropic exchange interaction. At the same time, interchain couplings are not exactly zero, but can be much smaller in comparison with intrachain interactions. In these so-called quasi-1D spin-chain materials, the interchain couplings can be treated as a small perturbation or are even negligible under certain conditions. In presence of the interchain couplings, the quasi-1D spin materials exhibit various interesting phenomena, such as a three-dimensional (3D) quantum phase transition [8, 18–20], confined spinon excitations [10, 11, 21–24], or the characteristic E_8 dynamical spectrum at a hidden 1D quantum critical point [10, 25–27]. As illustrated in figure 1, a 3D long-range order can be stabilized at finite temperature (T_{C} for ferromagnet and T_{N} for antiferromagnet). In an applied transverse magnetic field, the ordering temperature reduces continuously. A 3D quantum phase transition occurs at a critical field $B^{c,3\mathrm{D}}$ before the long-range order is completely suppressed.

At zero field, the spin dynamics of a Heisenberg-Ising (or XXZ) chain is characterized by fractionalized spinon excitations (or domain-wall excitations). Below the ordering temperature, the interchain couplings provide a confining potential to the spinon-pairs, because the interchain interactions are frustrated for the spins within the two spinons (or domain walls). The energy of the system increases linearly with the distance between the two spinons, thus the dynamics of a spinon-pair can be effectively described by the 1D Schrödinger equation [10, 11]

$$-\frac{\hbar^2}{\mu}\frac{d^2\varphi}{dx^2}+\lambda|x|\varphi=(E-2E_0)\varphi, \tag{1}$$

where $2E_0$ is the excitation energy threshold, $\lambda|x|$ is the linear confining potential due to interchain coupling with $\lambda=2B_{\parallel}\langle S^z\rangle/\tilde{c}$, and $\tilde{c}$ is the lattice constant. The solution features states with eigenenergies

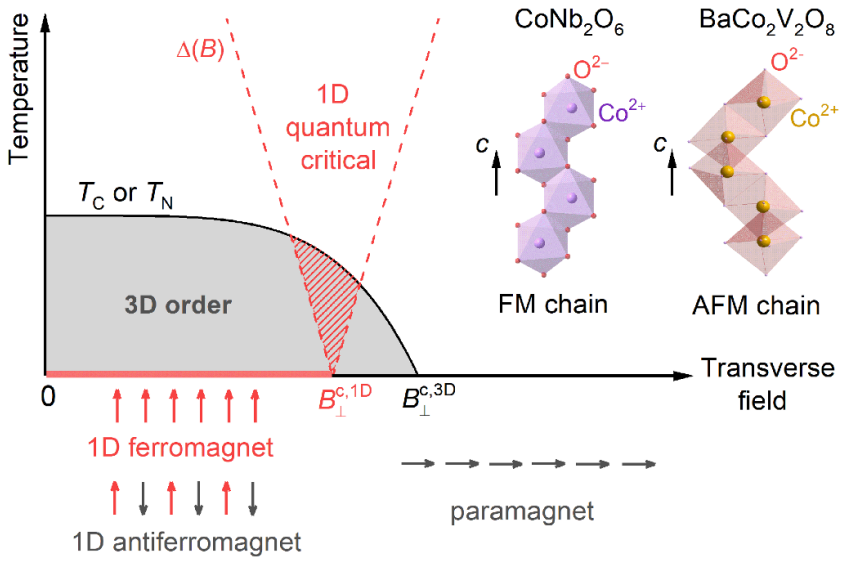

Figure 1. Schematic phase diagram of spin-1/2 one-dimensional and quasi-one-dimensional Ising-like magnets in an applied transverse magnetic field. Without interchain couplings a 1D Ising-like ferromagnet (FM) or antiferromagnet (AFM) exhibits a 1D long-range order only at zero temperature. With interchain couplings a 3D long-range order is formed at finite temperature below T_C or T_N for ferromagnet or antiferromagnet, respectively. The 1D and 3D long-range orders can be suppressed by an applied transverse field $B_\perp^{c,1D}$ or $B_\perp^{c,3D}$, respectively. Inset: a zigzag ferromagnetic spin chain of $CoNb_2O_6$ and a screw antiferromagnetic spin chain of $BaCo_2V_2O_8$ based on magnetic Co^{2+} ions [25, 27].

$$E_i = 2E_0 + \zeta_i \lambda^{2/3} \left(\frac{\hbar^2}{\mu}\right)^{1/3}, \qquad i = 1,2,3,\ldots, \tag{2}$$

which is a linear function of ζ_i, with ζ_i being the negative zeros of the Airy function, $\mathrm{Ai}(-\zeta_i) = 0$.

In general, one may treat small interchain couplings as an effective longitudinal magnetic field, and model a quasi-1D spin material by an effective 1D model Hamiltonian

$$\hat{H}_{\mathrm{FM}} = -J\sum_{\langle i,j\rangle} S_i^z S_j^z - B_\perp \sum_i S_i^x - B_\parallel \sum_i S_i^z, \tag{3}$$

where S_i denotes the spin on site i, $J>0$ is the nearest-neighbor exchange interaction for a ferromagnetic spin chain, and $\langle i,j\rangle$ indicates the summation over all pairs of nearest neighbors. $B_\perp$ denotes an applied transverse field. The effective fields due to the interchain coupling are longitudinal and denoted by $B_\parallel$. The corresponding Hamiltonian for an antiferromagnetic chain is found by performing a transformation $S_i \to (-1)^i S_i$, such that

$$\hat{H}_{\mathrm{AFM}} = J\sum_{\langle i,j\rangle} S_i^z S_j^z - B_\perp \sum_i S_i^x - (-1)^i B_\parallel \sum_i S_i^z, \tag{4}$$

with a staggered effective field $(-1)^i B_\parallel$.

Due to the effective fields $B_{\parallel}$, the systems exhibit a spin gap at $B_{\perp}^{c,1D} = J/2$, where otherwise a 1D transverse field Ising quantum critical point should occur. Around this perturbed quantum critical point, an integrable field theory was found, whose dynamical spectrum is described as corresponding to an E_8 Lie algebra [7, 28–30]. The dynamic spectrum is characterized by excitations of eight single quasiparticles and also continua of their multiple excitations. The energies of the eight quasiparticles are uniquely defined by their ratios. For instance, the ratio of the first two, $m_2/m_1 \approx 1.618$, is the golden ratio.

Previously, experimental studies suggested that the quasi-1D Ising-like ferromagnet $CoNb_2O_6$ [10, 20, 21, 27, 31, 32] and antiferromagnet $BaCo_2V_2O_8$ [9, 18, 22, 25, 26, 33] could be very good realizations of the Hamiltonians in equations (3) and (4), respectively. In this work, we perform terahertz (THz) absorption spectroscopy in an applied transverse magnetic field, and precisely track the evolution of the spin dynamics in these two compounds. Starting from zero-field confined spinons, the spin dynamics evolves through a characteristic E_8 dynamics, and finally exhibits a gap closing-reopening behavior, crossing the order-disorder phase boundary. These features are found to be sharply dependent on the THz radiation polarization relative to the spin chain direction, which appeals for further theoretical studies.

2. Experimental details

2.1. Magneto-THz spectroscopy of $BaCo_2V_2O_8$

The spin-chain antiferromagnet $BaCo_2V_2O_8$ orders below $T_N = 5.5$ K. Whereas the compound crystallizes in a tetragonal structure above T_N, a small orthorhombic distortion was found below T_N [18, 19]. The $BaCo_2V_2O_8$ single crystals were measured down to 2.7 K in a liquid-helium-bath cryostat, equipped with a superconducting magnet for applying fields up to 17 T. The intensity of THz radiation transmitted through the sample was measured with a bolometer, which was kept at 300 mK by a vacuum-insulated He-3 cooling circuit. The transmission spectra were recorded using a Martin–Puplett interferometer [34]. To study polarization dependence and field dependence of the spin excitations, we measured a $BaCo_2V_2O_8$ single crystal cut along the crystallographic *ac* plane both in Faraday and Voigt configurations, i.e. with the THz radiation travelling parallel and perpendicular to the applied magnetic field, respectively. In the following, we denote the in-plane tetragonal *a* axis by **a**, while the other equivalent tetragonal axis perpendicular to the sample surface will be denoted by **b**. The sample has a surface area of about $4 \times 4\,\mathrm{mm}^2$ and a thickness of 0.76 mm. We controlled the incident THz polarization using a rotating polarizer in front of the sample.

The absorption coefficient due to magnetic excitations is found by comparing the transmission spectra below T_N with a reference spectrum above T_N, for which we chose the zero-field transmission spectrum at 10 K. Since $BaCo_2V_2O_8$ undergoes a phase transition at T_N, the absorption peaks associated with the low-temperature phase are not present at 10 K. The absorption coefficient α is then equivalent to the differential absorbance

$$\alpha \equiv \Delta\alpha(B) = \alpha(B, 2.7\,\mathrm{K}) - \alpha(0\,\mathrm{T}, 10\,\mathrm{K}) = -\frac{1}{d}\ln\left[\frac{I(B, 2.7\,\mathrm{K})}{I(0\,\mathrm{T}, 10\,\mathrm{K})}\right], \tag{5}$$

where $I(B,T)$ is the transmitted intensity in a given field B at a given temperature T, and d denotes the sample thickness. For this insulator with relatively weak absorption peaks of

magnetic excitations, we assume the reflection coefficient to be constant in the given temperature range.

2.2. Magneto-THz spectroscopy of $CoNb_2O_6$

The spin-chain ferromagnet $CoNb_2O_6$ crystallizes in an orthorhombic structure with a long-range magnetic order formed below $T_C = 2.85$ K. A single crystal with a thickness of 0.5 mm and a diameter of about 3 mm was measured down to 250 mK in a He-3/He-4 dilution refrigerator with a 12 T superconducting magnet. For the detection of the THz radiation, a bolometer was cooled to 400 mK by a separate He-3 cooling circuit. A Martin–Puplett interferometer was utilized for the THz transmission experiment. The measurements were performed in Faraday configuration with an *ac*-cut sample, where the unpolarized light propagates along the *b* axis parallel to the applied magnetic field. With this experimental setup it was not feasible to perform measurements for Voigt configuration or with different THz polarizations.

Since warming up the sample above its ordering temperature in the dilution refrigerator is not attainable, we find the absorption coefficient by first calculating the differential absorbance at different magnetic field values using the zero-field spectrum at 250 mK as the reference. The differential absorbance is

$$\Delta\alpha(B) = \alpha(B) - \alpha(0\,\mathrm{T}) = -\frac{1}{d}\ln\left[\frac{I(B)}{I(0\,\mathrm{T})}\right], \tag{6}$$

where d is the sample thickness, and a constant reflection coefficient is once again assumed for this insulator. This, of course, introduces negative peaks at those frequencies where the absorption is present only in zero field. We then eliminate negative absorption and recover the zero-field absorption spectrum by subtracting a baseline from the differential absorbance, which gives us the absorption coefficient α. The subtracted baseline is obtained statistically from the median absorption values of all spectra measured at different strengths of the applied magnetic field.

In addition, we measured the same $CoNb_2O_6$ sample above T_C at 4 K by using a liquid-helium-bath cryostat. The sample was measured in the same configuration as in the dilution refrigerator, and the same procedure for calculating the absorption coefficient was utilized. In the liquid-helium-bath cryostat the rotating polarizer in front of the sample allowed us to measure the spectra with two orthogonal incident light polarizations.

3. Experimental results

3.1. Absorption spectra in $BaCo_2V_2O_8$

$BaCo_2V_2O_8$ crystallizes in a tetragonal structure with the spin chains running along the *c* axis. Figure 2 displays the absorption spectra of $BaCo_2V_2O_8$, measured at 2.7 K for various applied magnetic fields up to 17 T. The magnetic fields are applied perpendicular to the Ising axis (the *c* axis), with directions denoted by $\mathbf{B} \parallel \mathbf{a}$ or $\mathbf{B} \parallel \mathbf{b}$. These two orientations are equivalent because of the tetragonal crystalline structure. The spectra exhibit very clear polarization dependence. In zero field, a series of absorption peaks are only present when the THz oscillating magnetic field $\mathbf{B}^\omega$ is oriented along the *a* axis ($\mathbf{B}^\omega \parallel \mathbf{a}$, see figures 2(a) and (c)), while they completely disappear when $\mathbf{B}^\omega$ is along the *c* axis ($\mathbf{B}^\omega \parallel \mathbf{c}$, see figures 2(b) and (d)).

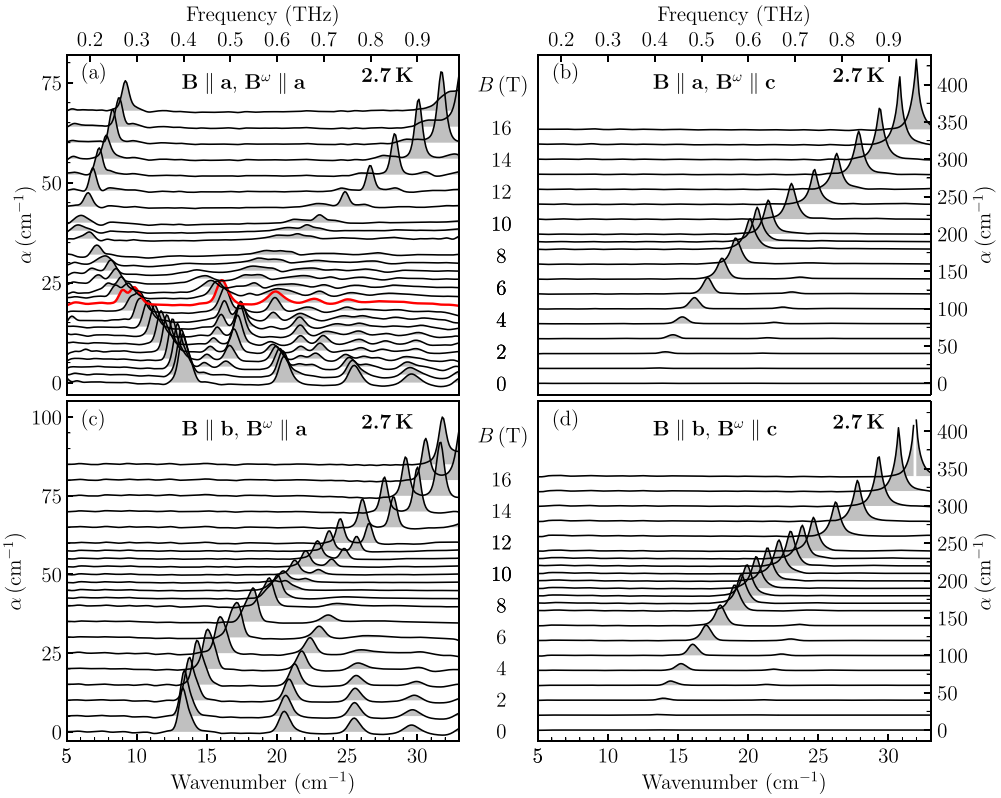

Figure 2. Magnetic-field dependence of the THz absorption spectrum of $BaCo_2V_2O_8$ measured at 2.7 K. The results from the Voigt measurements are presented in (a) for $\mathbf{B} \parallel \mathbf{a}$ and $\mathbf{B}^\omega \parallel \mathbf{a}$ and in (b) for $\mathbf{B} \parallel \mathbf{a}$ and $\mathbf{B}^\omega \parallel \mathbf{c}$. The data obtained from the Faraday configuration are shown in (c) for $\mathbf{B} \parallel \mathbf{b}$ and $\mathbf{B}^\omega \parallel \mathbf{a}$ and (d) for $\mathbf{B} \parallel \mathbf{b}$ and $\mathbf{B}^\omega \parallel \mathbf{c}$. The spectra are shifted upward proportionally to the values of the applied fields. The spectrum of $B_\perp^{c,1D} = 5$ T in (a) is highlighted in red.

In an applied magnetic field, the spectra of $\mathbf{B}^\omega \parallel \mathbf{c}$ are practically identical with the applied field directions $\mathbf{B} \parallel \mathbf{a}$ (figure 2(b)) and $\mathbf{B} \parallel \mathbf{b}$ (figure 2(d)). This also indicates that the a and b axes are equivalent in this material, as expected for the tetragonal structure. A single absorption peak is observed in the finite magnetic fields, which shifts to higher energy for higher fields and becomes increasingly stronger.

In contrast, the spectra of $\mathbf{B}^\omega \parallel \mathbf{a}$ are sensitive to the orientation of the applied magnetic field. As shown in figures 2(a) and (c), the spectra for $\mathbf{B} \parallel \mathbf{B}^\omega$ exhibit richer features than that of $\mathbf{B} \perp \mathbf{B}^\omega$, even though the THz polarization relative to the crystal axes is the same. For $\mathbf{B} \parallel \mathbf{B}^\omega \parallel \mathbf{a}$ (figure 2(a)), the zero-field modes split in finite fields. In particular, the lowest-lying mode softens with increasing field until 9.5 T, above which it hardens again. This is a signature of a field-induced quantum phase transition, which is consistent with the observed phase boundary at $B_\perp^{c,3D} = 9.5$ T between a low-field 3D ordered phase and high-field disordered phase [18], see figure 1. For $\mathbf{B} \perp \mathbf{B}^\omega \parallel \mathbf{a}$ (figure 2(c)), all the observed zero-field modes harden at higher magnetic fields. Above $B_\perp^{c,3D} = 9.5$ T, only the lowest-lying mode remains visible while the higher-energy modes disappear in the disordered phase. As we will discuss below,

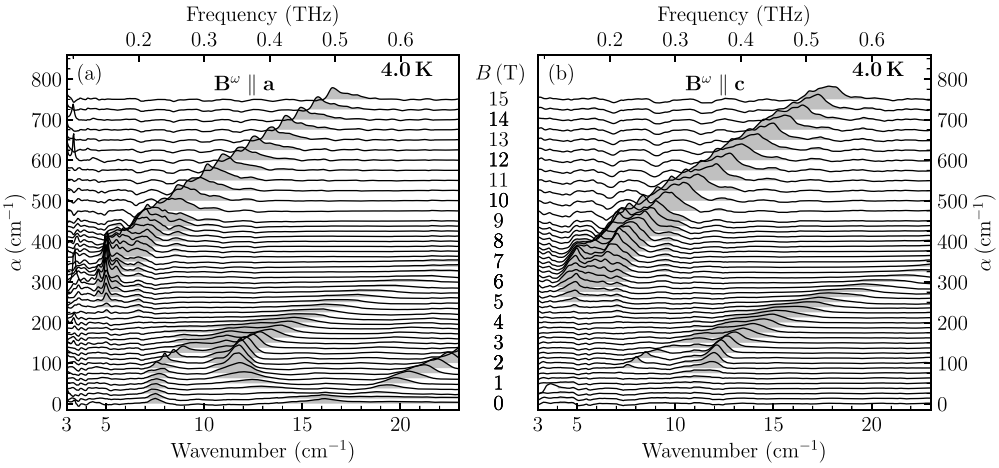

Figure 3. THz absorption spectra of $CoNb_2O_6$ at 4 K in applied magnetic fields along the *b* axis for polarizations (a) $\mathbf{B}^\omega \parallel \mathbf{a}$ and (b) $\mathbf{B}^\omega \parallel \mathbf{c}$. The spectra are shown every 0.25 T up to 12 T, and every 0.5 T up to 15 T.

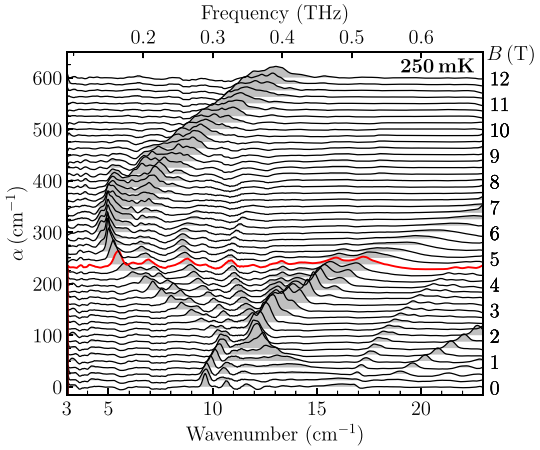

Figure 4. Unpolarized absorption spectra of $CoNb_2O_6$ at 250 mK in applied transverse fields up to 12 T. The spectrum at $B_\perp^{c,1D} = 4.75$ T is highlighted in red.

these higher-energy modes are the confined spinon excitations, which are present in the 3D ordered phase due to the interchain couplings.

3.2. Absorption spectra in $CoNb_2O_6$

The absorption spectra of $CoNb_2O_6$ above T_C and below T_C are presented in figures 3 and 4, respectively, for an applied transverse magnetic field along the crystallographic *b* axis. Above T_C, the spectra with two orthogonal polarizations are shown in figure 3(a) for $\mathbf{B}^\omega \parallel \mathbf{a}$ and in figure 3(b) for $\mathbf{B}^\omega \parallel \mathbf{c}$. In zero field, the $\mathbf{B}^\omega \parallel \mathbf{a}$ spectrum exhibits two modes at 7.5 and 16 cm^{-1}, while the spectrum of $\mathbf{B}^\omega \parallel \mathbf{c}$ is rather featureless. The energy of the 7.5 cm^{-1} mode

stays almost constant in the applied magnetic field until around 2 T, and then rapidly increases. In contrast, the 16 cm^{-1} mode splits into a softening and a hardening mode. Interestingly, the hardening branch is absent with $\mathbf{B}^{\omega} \parallel \mathbf{c}$, while the overall spectra above 2 T look very similar for the two polarizations. Above approximately 5 T, the spectra are mainly characterized by a rather broad absorption band, which shifts from 5 cm^{-1} to 17 cm^{-1} at 15 T. This band seems to be composed of more than one mode, which overlap with each other and can hardly be distinguished.

Figure 4 presents the spectra measured at 250 mK below T_C with unpolarized THz radiation for the transverse fields up to 12 T. In contrast to the spectra above T_C, the spectra of the magnetically ordered phase exhibit much richer features (see also figures 9(a) and (b)). There are more absorption peaks resolved, they are sharper and can be clearly followed in the applied magnetic fields. At higher fields above 5 T, the spectra are similar to those measured at 4 K, see figure 3.

4. Discussion

4.1. Confined spinons in the zero-field 3D ordered phases

The dynamics in a 1D quantum spin-1/2 magnet is characterized by fractionalized spinon excitations with a quantum number $S = 1/2$. A single spin-flip creates a pair of spinons, which could be viewed as two domain-walls. For a Heisenberg-Ising chain the spinon-pair excitations form a continuum with a spin-excitation gap. For a quasi-1D system below the ordering temperature, the spinons are confined in a linear potential due to the interchain couplings. The eigenenergies of the confined spinon excitations should follow the equation (2), featuring a linear dependence on ζ_i. The intercept $2E_0$ reflects the spin gap, which is due to the Ising anisotropy, while the slope $\lambda^{2/3}(\frac{\hbar^2}{\mu})^{1/3}$ contains the λ-term reflecting the strength of the confinement.

The zero field spectra of $BaCo_2V_2O_8$ below T_N and of $CoNb_2O_6$ below T_C were more concisely discussed previously in [25, 27], respectively, while they are represented here in figures 5 and 6 for further quantitative comparison. In the case of $BaCo_2V_2O_8$, a series of five absorption peaks is observed at $E_1 = 13.4$, $E_2 = 20.6$, $E_3 = 25.5$, $E_4 = 29.6$, and $E_5 = 33.1\,cm^{-1}$ (figure 5(a)). These frequencies are presented as a function of ζ_i for $i = 1, 2, \ldots, 5$ in figure 5(b), which exhibits clearly a linear dependence. A fit to the equation (2) provides $2E_0 = 5.73\,cm^{-1}$ ($\sim$0.71 meV) and $\lambda^{2/3}(\frac{\hbar^2}{\mu})^{1/3} = 3.51\,cm^{-1}$ ($\sim$0.44 meV). In the zero-field spectrum of $CoNb_2O_6$ at 250 mK, one can observe six modes at relatively lower frequencies, $E_1 = 9.6$, $E_2 = 10.7$, $E_3 = 11.6$, $E_4 = 12.6$, $E_5 = 13.4$, and $E_6 = 14.1\,cm^{-1}$ (figure 6(a)). The dependence of these frequencies on ζ_i, as shown in figure 6(b), follows also the linear function in equation (2), for the fit parameters $2E_0 = 7.97\,cm^{-1}$ ($\sim$0.99 meV) and $\lambda^{2/3}(\frac{\hbar^2}{\mu})^{1/3} = 0.68\,cm^{-1}$ ($\sim$0.084 meV).

The excellent linear fits show that the Schrödinger equation in equation (1) describes very well the observed excitations in $BaCo_2V_2O_8$ and in $CoNb_2O_6$, confirming the observation of confined spinons (or domain-wall excitations) in both compounds. The fit parameters are compared in figure 7, also with that of another spin-chain antiferromagnet $SrCo_2V_2O_8$ [11]. While the threshold energy in $CoNb_2O_6$ is the highest, the confining effect is least evident. In contrast, in $BaCo_2V_2O_8$ it requires the lowest energy to excite a spinon-pair, which experiences the largest confining among the three systems.

It is interesting to note that the confined spinons in $BaCo_2V_2O_8$ are absent in the spectrum if the polarized THz magnetic field is parallel to the Ising easy axis, i.e. $\mathbf{B}^{\omega} \parallel \mathbf{c}$ (see figures 2(b) and (d)), but are observed with $\mathbf{B}^{\omega}$ perpendicular to the easy axis (see figures 2(a) and (c)).

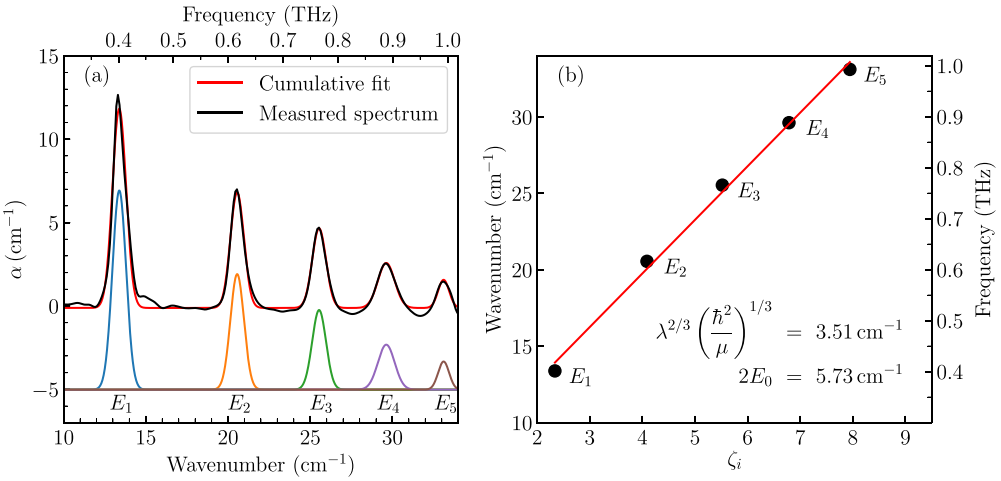

Figure 5. (a) Zero-field spectrum of $BaCo_2V_2O_8$ at 2.7 K below T_N. Fits of the five absorption peaks E_1–E_5 are shown under the spectrum. The red line shows the cumulative absorption from all five peaks. (b) Absorption peak energies, which follow a linear dependence on the negative zeros of the Airy function $A_i(-\zeta_i) = 0$ (see equation (2)). The linear fit parameters correspond to the linear confinement potential and the threshold energy for creating a spinon pair.

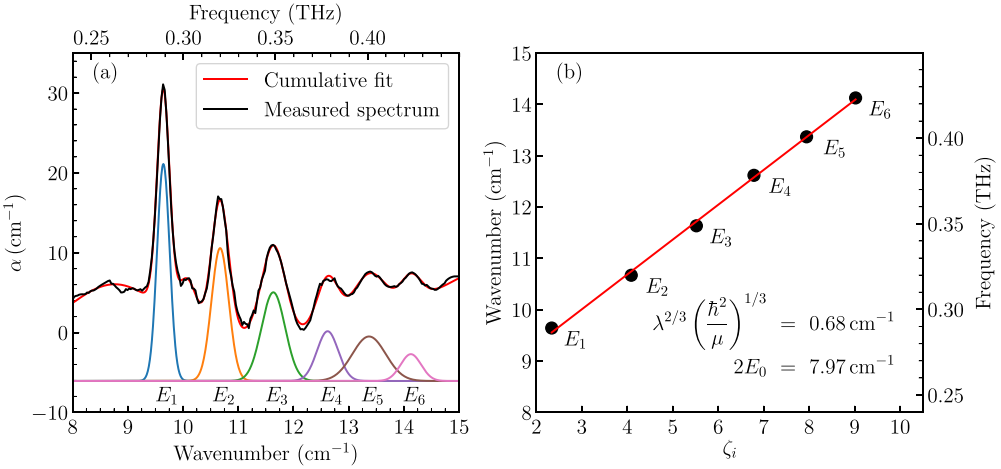

Figure 6. (a) Zero-field spectrum of $CoNb_2O_6$ at 250 mK below T_C. Fits of the six absorption peaks E_1–E_6 are shown under the spectrum. The red line shows the cumulative absorption, which includes the six peaks and a wide absorption background. (b) Absorption peak energies follow a linear dependence on ζ_i, the negative zeros of the Airy function $A_i(-\zeta_i) = 0$, for $2E_0 = 7.97\,\mathrm{cm}^{-1}$ and $\lambda^{2/3}(\frac{\hbar^2}{\mu})^{1/3} = 0.68\,\mathrm{cm}^{-1}$.

This can be understood as selection rule of magnetic-dipole excitations. In the 3D ordered phase, the spins are aligned antiferromagnetically along the c axis. Therefore, the coupling of the polarized THz magnetic field $\mathbf{B}^\omega$ with the spin component S_z will not trigger a spin-flip. A spin-flip excitation will occur when the THz magnetic field B^ω is along the transverse orientations, i.e. $\mathbf{B}^\omega \parallel \mathbf{a}$ or $\mathbf{B}^\omega \parallel \mathbf{b}$.

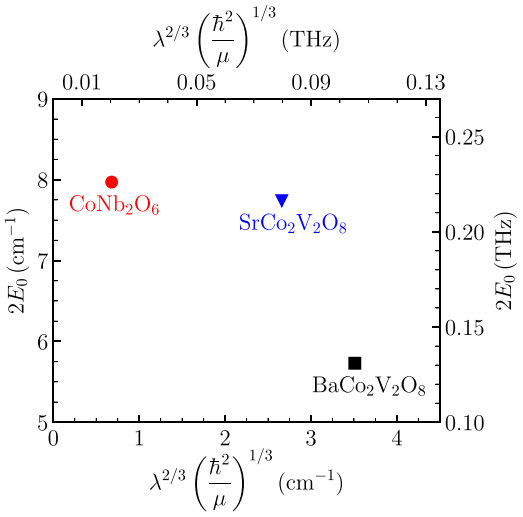

Figure 7. Threshold energy $2E_0$ versus linear confining potential $\lambda^{2/3}(\frac{\hbar^2}{\mu})^{1/3}$ for the confined spinons excited in $BaCo_2V_2O_8$, $CoNb_2O_6$, as well as $SrCo_2V_2O_8$ [11].

4.2. Spin dynamics in the transverse magnetic fields: E_8 characteristics and quantum phase transitions

4.2.1. $BaCo_2V_2O_8$. The field dependence of the observed spin excitations in $BaCo_2V_2O_8$ is represented in figure 8, where the resonance frequencies of the spin excitations are plotted as a function of the applied magnetic field. The spectra exhibit very clear contrast for different polarizations and for different orientations of the applied magnetic field, as compared in figures 8(a) and (b). While there are no excitations resolved in zero field for $\mathbf{B}^\omega \parallel \mathbf{c}$, a single mode is observed in a finite magnetic field above 2 T, which shifts to higher energy as the field is increased. The observation of this mode reflects that, in the applied transverse fields, the spins are tilted away from the c axis (the easy axis), which allows a spin-flip excitation through the coupling with the THz magnetic field. The field dependence of this mode is essentially identical to the one with the transverse fields applied along the a or the b axis, as a consequence of the pseudo-tetragonal symmetry.

While a quantitative understanding of the observed field-dependent behavior requires a detailed numerical calculation of the dynamical spectra, we highlight a few interesting observations. There is a clear contrast between two applied field directions $\mathbf{B} \parallel \mathbf{a}$ and $\mathbf{B} \parallel \mathbf{b}$ with the polarization $\mathbf{B}^\omega \parallel \mathbf{a}$. For $\mathbf{B}^\omega \perp \mathbf{B}$, the absorption modes corresponding to the confined spinons harden monotonically in the applied magnetic field, whereas for $\mathbf{B}^\omega \parallel \mathbf{B}$ these modes split in finite field and exhibit complex field-dependent evolutions (see figures 2(a) and 8(a)).

For $\mathbf{B}^\omega \parallel \mathbf{B} \parallel \mathbf{a}$, the lowest-lying mode softens continuously until about 9.5 T and then hardens monotonically in higher fields. This indicates a field-induced quantum phase transition at $B_\perp^{c,3D}$, above which the 3D order is suppressed as revealed by other experiments [9, 18]. At the same time, the higher-energy confined-spinon modes observed with $\mathbf{B} \parallel \mathbf{b}$ disappear above $B_\perp^{c,3D}$ as well. The lowest spinon-pair mode splits into two, with the lower-lying one exactly overlapping with the branch of $\mathbf{B}^\omega \parallel \mathbf{c}$ (see figure 8(b)).

In a different representation, figure 8(c), we plot the energy ratios of the higher-energy modes with respect to the lowest-lying mode m_1 for $\mathbf{B}^\omega \parallel \mathbf{B} \parallel \mathbf{a}$. We note that, between 4 and 6 T, a small satellite peak can be observed very close to the lowest-lying mode (see figure 2(a))

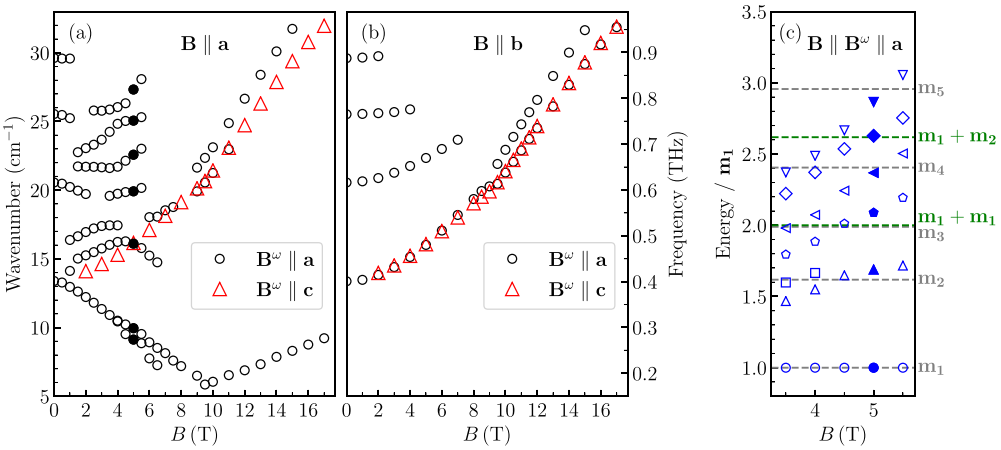

Figure 8. $BaCo_2V_2O_8$ absorption peak frequency dependence on the magnetic field at 2.7 K for the two field directions: (a) $\mathbf{B} \parallel \mathbf{a}$ and (b) $\mathbf{B} \parallel \mathbf{b}$. Solid black dots in (a) indicate the E_8 excitations at $B_\perp^{c,1D}$. (c) Ratios of the excitation energies with respect to the lowest-frequency excitation m_1 for the field direction $\mathbf{B} \parallel \mathbf{a}$ close to $B_\perp^{c,1D}$. The ratios approach theoretically predicted values for the E_8 excitations (marked with dashed lines) at 5 T. In (c) the frequency of m_1 is taken as the average of the two low-lying peaks, which split from a single peak due to anisotropy (see figure 2(a)).

Table 1. Selection rules for the observed confined spinons and E_8 excitations in $BaCo_2V_2O_8$ in a transverse magnetic field $\mathbf{B} \parallel \mathbf{a}$ or $\mathbf{B} \parallel \mathbf{b}$.

	$\mathbf{B} \parallel \mathbf{a}$ $\mathbf{B}^\omega \parallel \mathbf{c}$	$\mathbf{B} \parallel \mathbf{a}$ $\mathbf{B}^\omega \parallel \mathbf{a}$	$\mathbf{B} \parallel \mathbf{b}$ $\mathbf{B}^\omega \parallel \mathbf{c}$	$\mathbf{B} \parallel \mathbf{b}$ $\mathbf{B}^\omega \parallel \mathbf{a}$
confined spinons	no	yes	no	yes
E_8 excitations	no	yes	no	no

due to small magnetic anisotropy in the 3D ordered phase [18, 35]. Thus, in figure 8(c) the value of m_1 is taken as the average of the two low-lying peaks, which split from a single peak due to anisotropy. With increasing field, the ratios increase monotonically above 3 T. At 5 T, these ratios reach the expected ratios of the so-called E_8 particles (dashed lines) which was predicted for the perturbed 1D transverse-field Ising quantum critical point [7], corresponding to the Hamiltonians in equations (3) and (4) for ferromagnetic and antiferromagnetic chains, respectively. We can see that apart from the single-particle channel, the two-particle excitations $m_1 + m_2$ are also clearly observed. The observations for $\mathbf{B}^\omega \parallel \mathbf{B} \parallel \mathbf{a}$ were reported with a very good agreement with theoretical results [25, 30] and are also consistent with recent reports of inelastic neutron scattering [26].

The observed evolution of the spin dynamics from the confined spinons in zero field to the E_8 excitations at a perturbed 1D transverse-field Ising quantum critical point, which is also polarization dependent, is not straightforward to understand. The corresponding selection rules are summarized in table 1. Both the confined spinons and E_8 excitations are simultaneously allowed in only one configuration, $\mathbf{B}^\omega \parallel \mathbf{B} \parallel \mathbf{a}$. The observation of the E_8 excitations points to a realization of the phase diagram as illustrated in figure 1, i.e. the 1D quantum critical point is hidden in the 3D ordered phase, $B_\perp^{c,1D} < B_\perp^{c,3D}$. In the 3D ordered phase, the

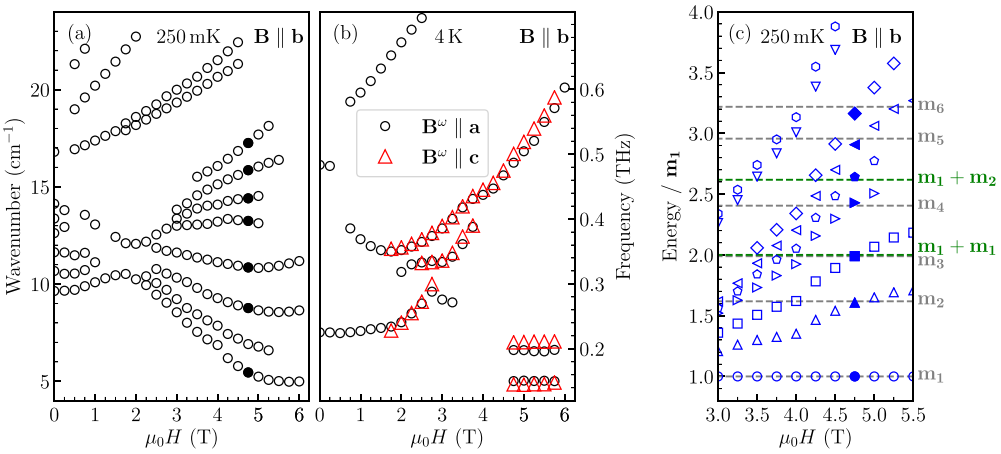

Figure 9. (a) $CoNb_2O_6$ absorption peak frequency dependence on the magnetic field $\mathbf{B} \parallel \mathbf{b}$ at 250 mK (see figure 4). Solid markers indicate the E_8 excitations at $B_\perp^{c,1D}$. (b) Resonance frequency as a function of the applied magnetic field at 4 K, which is above T_C. (c) Ratios of the excitation energies with respect to the lowest-frequency excitation m_1 for the field direction $\mathbf{B} \parallel \mathbf{b}$ close to $B_\perp^{c,1D}$ (see black dots in (a)). The ratios approach theoretically predicted values for the E_8 excitations (marked with dashed lines) at 4.75 T.

interchain couplings provide the required perturbative longitudinal field for the emergence of the E_8 excitations.

4.2.2. $CoNb_2O_6$. A similar phase diagram is also realized in the ferromagnetic chain $CoNb_2O_6$. As shown in figures 4 and 9(a), the lower-lying confined-spinon modes harden while the higher-lying ones soften in the applied transverse field. Above 2 T, these modes exhibit different field dependencies. The overall field dependence of the spin excitation spectra is not the same as in $BaCo_2V_2O_8$. This shows that the observed field-dependent behavior is not universal but material-dependent, and a quantitative description, therefore, requires a material- or model-specific numerical analysis. Nonetheless, we can see that, above 2 T, the lowest-energy mode softens continuously until a critical field $B_\perp^{c,3D} \approx 5.3$ T for $CoNb_2O_6$, which is followed by hardening in higher fields (see also figure 4). This corresponds to the suppression of the 3D ordered phase by the applied magnetic field, which is consistent with previous reports [20]. Approaching the critical field from below, the energy ratios with respect to the lowest-lying mode exhibit a monotonic increase. At $B_\perp^{c,1D} = 4.75$ T, these ratios simultaneously reach the expected ratios of the E_8 excitations up to the energy of the sixth particle m_6 (figure 9(c)) [27]. This not only confirms the observation of the E_8 excitations beyond the energy of $2m_1$ [36], but also demonstrates the material-independent universality of the E_8 dynamics characteristic of the perturbed 1D transverse-field Ising quantum critical point.

5. Summary

We have performed THz spectroscopy of quantum spin dynamics in the quasi-one-dimensional spin-1/2 Ising-like antiferromagnet $BaCo_2V_2O_8$ and ferromagnet $CoNb_2O_6$ in applied transverse magnetic fields. Due to interchain couplings, 3D ordering phases are formed below

$T_N = 5.5\,\mathrm{K}$ for $BaCo_2V_2O_8$ and below $T_C = 2.85\,\mathrm{K}$ for $CoNb_2O_6$. In zero field, the spin dynamics is characterized by confined-spinon (domain-wall) excitations. With increasing magnetic field, the systems evolve in material-dependent complex ways through a regime where a characteristic E_8 dynamical spectrum is observed (around 5 T for $BaCo_2V_2O_8$ and 4.75 T for $CoNb_2O_6$), and finally enter the field-induced disordered phase above the 3D quantum critical field $B_\perp^{c,3D}$ (9.5 T for $BaCo_2V_2O_8$ and 5.3 T for $CoNb_2O_6$). Moreover, we determine the polarization dependence of the confined-spinon excitations and the E_8 excitations in $BaCo_2V_2O_8$. While the detected confined spinons reflect material-dependent magnetic properties, the observed E_8 dynamical spectrum exhibits universal characteristics of a perturbed 1D transverse-field Ising quantum critical point. Beyond the critical regime, a quantitative understanding of the field-dependent spin dynamics remains a subject for further theoretical studies.

Data availability statement

The data that support the findings of this study are available upon reasonable request from the authors.

Acknowledgments

We thank Jianda Wu and Zhao Zhang for very helpful discussions. We acknowledge support by personal research funding grant PRG736 of the Estonian Ministry of Education and Research, by European Regional Development Fund Project No. TK134., by the DFG (German Research Foundation) via the Project No. 277146847—Collaborative Research Center 1238: Control and Dynamics of Quantum Materials (Subprojects No. A02, B01, and B05), and by the the European Research Council (ERC) under the Horizon 2020 research and innovation programme, Grant Agreement No. 950560 (DynaQuanta).

ORCID iDs

Johannes Engelmayer https://orcid.org/0000-0002-3454-1601
Zhe Wang https://orcid.org/0000-0001-7464-5408

References

[1] Pfeuty P 1970 The one-dimensional Ising model with a transverse field *Ann. Phys.* **57** 79–90
[2] Sachdev S 1999 *Quantum Phase Transitions* (New York: Cambridge University Press)
[3] Suzuki S, Inoue J and Chakrabarti B K 2013 *Quantum Ising Phases and Transitions in Transverse Ising Models* (Heidelberg: Springer GmbH)
[4] Dutta A, Aeppli G, Chakrabarti B K, Divakaran U, Rosenbaum T F and Sen D 2015 *Quantum Phase Transitions in Transverse Field Spin Models: From Statistical Physics to Quantum Information* (Cambridge: Cambridge University Press)
[5] Mussardo G 2009 *Statistical Field Theory: An Introduction to Exactly Solved Models in Statistical Physics* (Oxford: Oxford Graduate Texts, Oxford University Press)
[6] Giamarchi T 2003 *Quantum Physics in One Dimension* (Oxford: Oxford University Press)
[7] Zamolodchikov A B 1989 Integrals of motion and *S*-matrix of the (scaled) $T = T_c$ Ising model with magnetic field *Int. J. Mod. Phys.* A **04** 4235–48
[8] Wang Z *et al* 2018 Quantum criticality of an Ising-like spin-1/2 antiferromagnetic chain in a transverse magnetic field *Phys. Rev. Lett.* **120** 207205

[9] Faure Q *et al* 2018 Topological quantum phase transition in the Ising-like antiferromagnetic spin chain $BaCo_2V_2O_8$ *Nat. Phys.* **14** 716
[10] Coldea R, Tennant D A, Wheeler E M, Wawrzynska E, Prabhakaran D, Telling M, Habicht K, Smeibidl P and Kiefer K 2010 Quantum criticality in an Ising chain: experimental evidence for emergent E_8 symmetry *Science* **327** 177–80
[11] Wang Z, Schmidt M, Bera A K, Islam A T M N, Lake B, Loidl A and Deisenhofer J 2015 Spinon confinement in the one-dimensional Ising-like antiferromagnet $SrCo_2V_2O_8$ *Phys. Rev.* B **91** 140404
[12] Wang Z *et al* 2016 From confined spinons to emergent fermions: observation of elementary magnetic excitations in a transverse-field Ising chain *Phys. Rev.* B **94** 125130
[13] Wang Z *et al* 2018 Experimental observation of Bethe strings *Nature* **554** 219–23
[14] Bera A K *et al* 2020 Dispersions of many-body Bethe strings *Nat. Phys.* **16** 625–30
[15] Lenz W 1920 Beitrag zum Verständnis der magnetischen Erscheinungen in festen Körpern *Phys. Z.* **21** 613–15
[16] Ising E 1925 Beitrag zur Theorie des Ferromagnetismus *Z. Phys.* **31** 253–8
[17] Brush S G 1967 History of the Lenz-Ising model *Rev. Mod. Phys.* **39** 883–93
[18] Niesen S K, Kolland G, Seher M, Breunig O, Valldor M, Braden M, Grenier B and Lorenz T 2013 Magnetic phase diagrams, domain switching and quantum phase transition of the quasi-one-dimensional Ising-like antiferromagnet $BaCo_2V_2O_8$ *Phys. Rev.* B **87** 224413
[19] Niesen S K, Breunig O, Salm S, Seher M, Valldor M, Warzanowski P and Lorenz T 2014 Substitution effects on the temperature versus magnetic field phase diagrams of the quasi-one-dimensional effective Ising spin-12 chain system $BaCo_2V_2O_8$ *Phys. Rev.* B **90** 104419
[20] Liang T, Koohpayeh S M, Krizan J W, McQueen T M, Cava R J and Ong N P 2015 Heat capacity peak at the quantum critical point of the transverse Ising magnet $CoNb_2O_6$ *Nat. Commun.* **6** 7611
[21] Morris C M, Valdés Aguilar R, Ghosh A, Koohpayeh S M, Krizan J, Cava R J, Tchernyshyov O, McQueen T M and Armitage N P 2014 Hierarchy of bound states in the one-dimensional ferromagnetic Ising chain $CoNb_2O_6$ investigated by high-resolution time-domain terahertz spectroscopy *Phys. Rev. Lett.* **112** 137403
[22] Grenier B, Petit S, Simonet V, Canévet E, Regnault L-P, Raymond S, Canals B, Berthier C and Lejay P 2015 Longitudinal and transverse Zeeman ladders in the Ising-like chain antiferromagnet $BaCo_2V_2O_8$ *Phys. Rev. Lett.* **114** 017201
[23] Morris C M *et al* 2021 Duality and domain wall dynamics in a twisted Kitaev chain *Nat. Phys.* **17** 832–6
[24] Rutkevich S B 2022 Spinon confinement in the gapped antiferromagnetic XXZ spin-12 chain *Phys. Rev.* B **106** 134405
[25] Zhang Z *et al* 2020 Observation of E_8 particles in an Ising chain antiferromagnet *Phys. Rev.* B **101** 220411
[26] Zou H *et al* 2021 E_8 spectra of quasi-one-dimensional antiferromagnet $BaCo_2V_2O_8$ under transverse field *Phys. Rev. Lett.* **127** 077201
[27] Amelin K, Engelmayer J, Viirok J, Nagel U, Rõõm T, Lorenz T and Wang Z 2020 Experimental observation of quantum many-body excitations of E_8 symmetry in the Ising chain ferromagnet $CoNb_2O_6$ *Phys. Rev.* B **102** 104431
[28] Delfino G and Mussardo G 1995 The spin-spin correlation function in the two-dimensional Ising model in a magnetic field at $T = T_c$ *Nucl. Phys.* B **455** 724–58
[29] Oshikawa M 2020 Experimental observations of the universal cascade of bound states in quantum Ising chain in a magnetic field and E_8 symmetry *J. Club Condens. Matter Phys.* (https://doi.org/10.36471/JCCM_September_2020_04)
[30] Wang X, Zou H, Hódsági K, Kormos M, Takács G and Wu J 2021 Cascade of singularities in the spin dynamics of a perturbed quantum critical Ising chain *Phys. Rev.* B **103** 235117
[31] Husson E, Repelin Y, Dao N Q and Brusset H 1977 Characterization of different bondings in some divalent metal niobates of columbite structure *Mater. Res. Bull.* **12** 1199–206
[32] Kinross A W, Fu M, Munsie T J, Dabkowska H A, Luke G M, Sachdev S and Imai T 2014 Evolution of quantum fluctuations near the quantum critical point of the transverse field Ising chain system $CoNb_2O_6$ *Phys. Rev.* X **4** 031008
[33] Kimura S, Okunishi K, Hagiwara M, Kindo K, He Z, Taniyama T, Itoh M, Koyama K and Watanabe K 2013 Collapse of magnetic order of the quasi one-dimensional Ising-like antiferromagnet $BaCo_2V_2O_8$ in transverse fields *J. Phys. Soc. Japan* **82** 033706

[34] Wang Z, Reschke S, Hüvonen D, Do S-H, Choi K-Y, Gensch M, Nagel U, Rõõm T and Loidl A 2017 Magnetic excitations and continuum of a possibly field-induced quantum spin liquid in α-$RuCl_3$ *Phys. Rev. Lett.* **119** 227202

[35] Okutani A, Kimura S, Takeuchi T and Hagiwara M 2015 High-field multi-frequency ESR in the quasi-1D $S = 1/2$ Ising-like antiferromagnet $BaCo_2V_2O_8$ in a transverse field *Appl. Magn. Reson.* **46** 1003–6

[36] Kjäll J A, Pollmann F and Moore J E 2011 Bound states and E_8 symmetry effects in perturbed quantum Ising chains *Phys. Rev.* B **83** 020407